Appl Phys A (2010) 101: 539–544
DOI 10.1007/s00339-010-5893-8

Applied Physics A
Materials Science & Processing

Assessment of laser-induced thermal load on silicon nanostructures based on ion desorption yields

Bennett N. Walker · Jessica A. Stolee · Deanna L. Pickel · Scott T. Retterer · Akos Vertes

Received: 17 November 2009 / Accepted: 24 May 2010 / Published online: 10 July 2010

Abstract Experimental assessment of the thermal load induced by fast laser pulses on micro- and nanostructures through IR imaging is currently too slow and lacks the spatial resolution to be useful. In this paper, we introduce a method based on measuring the laser-induced yields of ions to compare the thermal loads on nanofabricated silicon structures, when exposed to nanosecond laser pulses. The laser fluences at which the ion yields of, for example, sodiated and potassiated peptides ions are equal for two different structures correspond to equivalent thermal loads. Using alkalinated peptides is a convenient choice because the corresponding ion intensities are easily measured up to the melting point of silicon. As an example, we compare the nanosecond laser heating of silicon nanopost arrays with diverse post diameters and periodicities. Assessment of the thermal load through ion yield measurements can also be used to verify model assumptions for heat transport regimes in nanostructures.

1 Introduction

As the dimensions of semiconductor structures in electronic devices are reduced, the importance of energy dissipation and heat conduction increases. Due to their physical dimensions, surface temperature measurements on nanostructures are challenging and make the comparison of the thermal load on different structures difficult. Currently, IR imaging is unable to achieve the spatial resolution sufficient for nanostructures (the best available spatial resolution is ∼10 μm) [1]. Likewise, the temporal resolution of IR cameras (currently ∼200 μs) [2] is insufficient to follow the changes induced on the nanosecond timescale. In the case of exposure to short or ultrashort laser pulses, the transient nature of the heating process makes assessing the thermal load on these structures a trial and error process. The ultimate indicator of excessive heating is the melting of the structure that can be detected after the fact using, e.g., scanning electron microscopy (SEM).

Currently the only way to assess the thermal load on sub-micrometer length and sub-microsecond timescale is through model calculations. However, modeling surface temperatures at these conditions can be challenging. As the dimensions of the structure approach the phonon mean free path, approximately 800 nm for silicon at room temperature [3], heat transport is no longer purely diffusive and is more accurately described by the Boltzmann equation [4, 5]. Furthermore, at nanoscopic dimensions the thermal conductivity of silicon is significantly reduced compared to the values observed for the bulk material [6, 7]. Thus, the equations governing the heat dissipation in complex nanostructures vary according to the dimensions of the structure and the prediction of the thermal load becomes challenging for all but the simplest geometries.

Heating of solid surfaces can result in the desorption of adsorbates and the emission of ions. In a vacuum environment, these ions can be mass analyzed and the detected ion intensities correlate with the surface temperatures. For example, in stationary heating experiments, the rate coefficients for the desorption of Cs^+ and K^+ from hot metal surfaces follow the Arrhenius law [8], in some cases, for over

B.N. Walker · J.A. Stolee · A. Vertes (✉)
Department of Chemistry, George Washington University, Washington, DC 20052, USA
e-mail: vertes@gwu.edu

D.L. Pickel · S.T. Retterer
Center for Nanophase Materials Sciences, Oak Ridge National Laboratory, Oak Ridge, TN 37831, USA

five orders of magnitude [9]. Transient laser heating of surfaces and nanostructures also produces alkaline ions. However, to determine the critical thermal load on silicon, temperatures close to the melting point, 1687 K, are required. At these temperatures, the signal from alkaline ions becomes saturated. In gas phase ion molecule reactions, these ions also react with molecular adsorbates to produce quasimolecular ions [10, 11]. The intensity of these quasimolecular ions is significantly lower and results in an extended dynamic range and scales with the surface temperature of the nanostructure close to the melting point.

When a pulsed laser irradiates a structure, energy is deposited into the silicon that can heat it to high temperatures, potentially resulting in structural failure. For example, in the case of nanopost arrays (NAPA) structures the silicon nanoposts absorb the laser radiation and undergo transient heating. If the temperature reaches the melting point of silicon, the posts are deformed or destroyed. At lower laser fluences, the excitation of the structure results in the removal of surface monolayers by transferring material from the solid phase to the vapor phase, leaving no visible damage [12]. If a trace amount of a non-absorbing adsorbate is deposited onto the structure and exposed to laser radiation some of it will be transferred into the vapor phase and ionized. Due to the low quantities of the adsorbate, there is a negligible effect on the deposition and redistribution of the laser pulse energy.

In this contribution we demonstrate that depositing trace amounts of peptide adsorbates on silicon NAPA [13] of different post diameters and periodicities and measuring the quasimolecular ion yields in response to a laser pulse can be used to assess the relative surface temperatures of the nanostructure. Based on this simple thermal load indicator, a quick comparison of nanosecond-scale energy dissipation by different structures becomes possible.

2 Experimental

2.1 Materials

Mechanical grade boron doped p-type silicon wafers of 280 ± 20 μm thickness and 0.001–100 Ω cm resistivities were purchased from University Wafer (South Boston, MA). The following three neuropeptides were used: substance *P* acetate salt hydrate (Arg-Pro-Lys-Pro-Gln-Gln-Phe-Phe-Gly-Leu-Met-NH_2), bradykinin (Arg-Pro-Pro-Gly-Phe-Ser-Pro-Phe-Arg) and leucine enkephalin (Tyr-Gly-Gly-Phe-Leu), and HPLC grade water and methanol were purchased from Sigma-Aldrich (St. Louis, MO). Although the neuropeptides were of >95% purity, they contained sufficient amount of alkali ions to prevent the depletion of alkali in the laser desorption experiments.

2.2 NAPA production

Posts with specific diameters between 100 nm and 250 nm, periodicities of 337 nm or 674 nm and heights of ∼1000 nm were nanofabricated on the silicon wafers using e-beam lithography (JBX-9300, JEOL, Peabody, MA) and reactive ion etching (PlasmaLab100 reactive ion etching system, Oxford, Oxfordshire, UK). To maintain similar trough widths for the thinner posts with diameters between 100 nm and 150 nm and the thicker posts with diameters between 175 nm and 250 nm, the periodicities were selected as 337 nm and 674 nm, respectively.

Briefly, in the fabrication process, first the ZEP250A resist was spin coated onto the silicon wafer and, using e-beam lithography, the desired nanopost pattern was developed through resist softening. The exposed resist was removed in a xylenes bath and the wafer was descummed to prepare it for masking. Next, using an electron beam evaporator, a ∼100 Å thick chromium layer was deposited onto the silicon wafer at a rate of 0.1 nm/s. The remainder of the resist along with excess chromium was removed through sonication in baths of acetone and isopropyl alcohol, leaving only the chromium discs at the intended location of the posts on the wafer. Finally, the nanoposts were produced via reactive ion etching at a rate of ∼100 nm/min using a combination of C_4F_8, SF_6 and Ar plasma gases. The desired heights were produced by adjusting the etching time. The resulting NAPA were then inspected with an SEM (Nova Nanolab 600 DualBeam™ system, FEI, Hillsboro, OR) to confirm their integrity and dimensions. As an example, Fig. 1a shows an SEM image of NAPA with a post height and diameter of 1000 nm and 150 nm, respectively.

2.3 Mass spectrometry

Laser desorption ionization time-of-flight mass spectrometry experiments were conducted on the NAPA structures with peptide adsorbates. The experimental geometry was identical to the one described in Reference [13]. A small volume (0.5 μL) of the 200 μM aqueous solution was deposited onto the surface and air dried. The NAPA structure was inserted into a time-of-flight mass spectrometer (Kratos Axima III, Shimadzu-Kratos, Manchester, UK) with a nitrogen laser source (337 nm wavelength) and a curved field reflectron. Mass spectra were acquired (see Fig. 1b) as a function of laser fluence and ion yields were determined by integrating the areas of the quasimolecular ion peaks using the Origin 7 scientific visualization package (OriginLab Corporation; Northampton, MA).

2.4 Temperature distribution modeling

The surface temperature distributions of individual nanoposts during exposure to pulsed laser irradiation were modeled using the FlexPDE 6.0 finite difference package (PDE

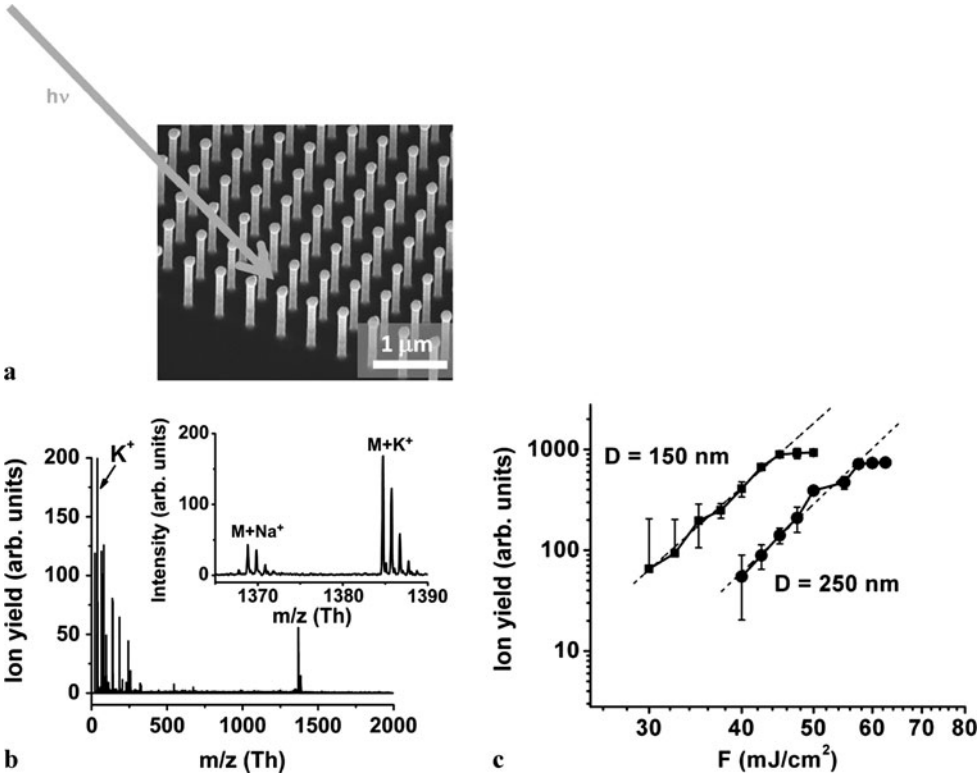

Fig. 1 (**a**) Scanning electron microscope image of NAPA segment with $D = 150$ nm, $H = 980$ nm and $P = 450$ nm, (**b**) laser desorption ionization mass spectrum of substance P from this substrate as well as the saturated K^+ peak. The *inset* shows the spectrum zoomed to show the quasimolecular ions. (**c**) Substance P ion yields as a function of laser fluence for $H = 1000$ nm posts with $D = 150$ nm (■) and 250 nm (●) diameter. The periodicities for the thinner posts ($D = 150$ nm) was $P = 337$ nm, whereas for the thicker posts ($D = 250$ nm) was $P = 674$ nm. The slopes for the linear segments of the logarithmic plots were 6.6 ± 0.8 for $D = 150$ nm, and 7.0 ± 0.5 for $D = 250$ nm posts, indicating a strongly nonlinear process

Solutions Inc.; Spokane Valley, WA). For systems with large changes in the temperature, in the Fourier law the heat flux vector, $\boldsymbol{q}$, is described as $\boldsymbol{q} = -\kappa(T)\nabla T$, where $\kappa(T)$ is the temperature-dependent thermal diffusivity, and T is the temperature distribution. Under these circumstances, the temperature distribution in the NAPA structure induced by a polarized laser pulse impinging under the angle of incidence, θ, is defined by:

$$\frac{\partial T}{\partial t} = \nabla\big(\kappa(T)\nabla T\big) + (1-R)\frac{\alpha V}{C_p} I_i(x,y,t)\sin^2\theta\cos^2\varphi \times \exp(-\alpha z), \quad (1)$$

where R and C_p are the temperature-dependent reflectivity and specific heat, whereas V, φ, I_i, and α are the molar volume, angle of polarization, laser irradiance and absorption coefficient, respectively [14]. The angle of polarization is measured between the plane of the electric field vector and the post axes.

Equation (1) was solved for insulating boundary conditions (except for the base of the post, where conductive heat loss was allowed) and using the material parameters for silicon. Experimental values for temperature-dependent mesoscopic thermal conductivity [15] and reflectivity [16] were fitted by polynomials and introduced into the model. The calculations compared the exposure of different silicon nanoposts to nitrogen laser pulses of 5 ns length and fluences between 10 and 100 mJ/cm^2.

3 Results and discussion

3.1 Laser desorption ionization mass spectrometry

Trace amounts of substance P were deposited onto the NAPA structures and the ion yields of the quasimolecular ions (MH^+, MNa^+ and MK^+) for this molecule, M, were measured as a function of the applied laser fluence, F. Results for the other two neuropeptides were similar but only substance P is discussed here. Above a threshold, the ion yields grew rapidly as the fluence of the desorption laser was increased (see Fig. 1c). The slopes for the linear segments of the logarithmic plots were 6.6 ± 0.8 for $D = 150$ nm, and 7.0 ± 0.5 for $D = 250$ nm posts, indicating a strongly nonlinear process. At higher fluences, the ion yield curves reached saturation that was accentuated by noticeable but very limited ion fragmentation. Assuming that a given ion yield corresponds to a certain thermal load, it is clear from Fig. 1c that the same thermal load for larger diameter posts is reached at higher fluences. This is consistent with our observations indicating that thinner posts were damaged at lower laser fluences. The correlation between the applied fluence and the ion yield was used to gauge the relative surface temperatures on a given structure.

Inspection of the sodiated and potassiated molecular ion intensities (see the inset of Fig. 1b) revealed that at low fluences the sodiated ions were more abundant, whereas at high fluences the potassiated ion intensities were higher. Sim-

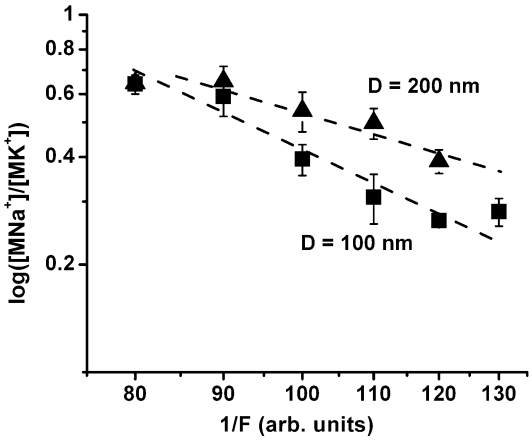

Fig. 2 For $H = 1000$ nm posts with $D = 100$ nm and $P = 337$ nm (■), and $D = 200$ nm and $P = 674$ nm (▲), the correlation between the logarithm of the $[MNa^+]/[MK^+]$ intensity ratio and the inverse of the laser fluence showed linearity over the studied fluence range with $r = 0.96$ and $r = 0.91$ correlation coefficients, respectively

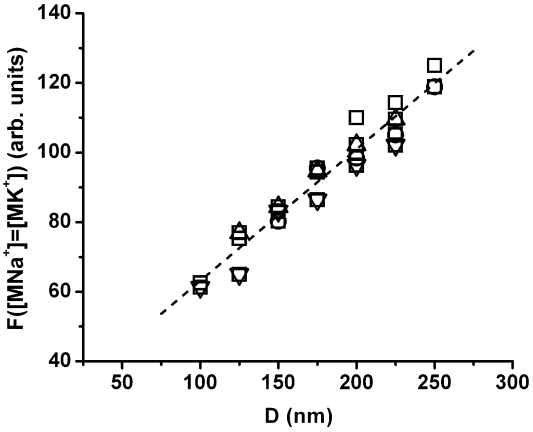

Fig. 3 Fluence required to reach equal abundances for the sodiated and potassiated substance P ion, $[MNa^+] = [MK^+]$, as a function of nanopost diameter, D, for NAPA structures with different resistivities. The silicon wafers used to produce the NAPA were selected from batches in the 0.001–0.005 Ω cm (□), 1–5 Ω cm (○), 5–10 Ω cm (△), and 10–100 Ω cm (▽) resistivity ranges. The posts were $H = 1000$ nm high and their periodicities were $P = 337$ nm for 100 nm $\leq D \leq$ 150 nm and $P = 674$ nm for 175 nm $\leq D \leq$ 250 nm. The linear regression line had a correlation coefficient of $r = 0.97$

ilar observations had been made for laser desorption ionization from laser-induced silicon microcolumn arrays [17]. For NAPA the intensity ratio $[MNa^+]/[MK^+]$ decreased as a function of the fluence. An Arrhenius-type plot for the logarithm of the intensity ratio and the inverse of the fluence indicated linearity throughout the studied range (see Fig. 2). The linear regression lines for the $D = 100$, 150, 200 and 250 nm systems exhibited an average slope of $b = -0.012 \pm 0.003$.

These observations are consistent with a simple kinetic model of alkaline ion production from the silicon impurities and ion molecule reactions between these alkali ions and the adsorbate molecules. Assuming a simple activation process that follows zero-order kinetics, the concentration of sodium ions by the end of a laser pulse of t_p length can be expressed as:

$$\left[Na^+\right]_0 = k_0 t_p = A_{Na^+} \exp\left[-\frac{\Delta E_{Na^+}}{kT}\right] t_p, \tag{2}$$

where k_0 is the rate coefficient, and A_{Na^+} and ΔE_{Na^+} are the frequency factor and the activation energy of the sodium ion emission, respectively. A similar equation is valid for the $[K^+]_0$ potassium ion intensities.

If the adsorbate molecules are present in a large surplus, $[M] \gg [Na^+]_0$ and $[M] \gg [K^+]_0$, the production of the alkalinated quasimolecular ions follow the pseudo-first order kinetics. As a result, the ratio of the sodiated and potassiated molecular ion concentrations, x, in the plume is described as:

$$x = \frac{[MNa^+]}{[MK^+]} = \frac{[Na^+]_0 (1 - e^{-k_{Na^+} t})}{[K^+]_0 (1 - e^{-k_{K^+} t})}, \tag{3}$$

where k_{Na^+} and k_{K^+} are the pseudo-first order rate coefficients for the ion molecule reactions and t is the reaction time defined by the residence of these ions in the source region. In case the exponents in (3) are close to zero and (2) is introduced, the expression simplifies to:

$$A_{Na^+} \exp\left[-\frac{\Delta E_{Na^+}}{kT_x}\right] k_{Na^+} = x A_{K^+} \exp\left[-\frac{\Delta E_{K^+}}{kT_x}\right] k_{K^+}. \tag{4}$$

In the absence of a permanent dipole moment, the cationization rate of a large molecule with polarizability, α_{pol}, by a small ion, e.g., sodium, is $k_{Na^+} = 2\pi e \sqrt{\alpha_{pol}/M_{Na^+}}$, where M_{Na^+} is the molecular mass of sodium [18]. After substituting these rate coefficients into (4) and rearranging it we arrive to:

$$\ln \frac{[MNa^+]}{[MK^+]} = \frac{\Delta E_{K^+} - \Delta E_{Na^+}}{kT_x} - \ln\left(\frac{A_{K^+}}{A_{Na^+}} \sqrt{\frac{M_{Na^+}}{M_{K^+}}}\right). \tag{5}$$

Thus the ratio of quasimolecular ion intensities as a function of temperature, indeed, follows the Arrhenius expression. Assuming a linear relationship between the incident laser fluence and the surface temperature, which holds for a uniform penetrating source (see e.g., [14]), (5) describes the findings in Fig. 2.

According to our assumption, the advantage of gauging the surface temperature through ion yield ratios is that we can compare nanostructures without introducing considerations for the heat transport mechanism. To further explore this hypothesis, we compared the ion yield ratios from NAPA structures of different post diameters and electrical resistivities. Figure 3 shows the laser fluence, F, required to reach $[MNa^+] = [MK^+]$ as a function of post diameter

for resistivities spanning over four orders of magnitude. Irrespective of the resistivity, the data indicates an apparent linear relationship between these quantities with a correlation coefficient of $r = 0.97$. This is significant because silicon wafers with a wide range of resistivities are used for the fabrication of nanostructures. The method introduced here seems to work independent of the direct current resistivity.

The relationship established in Fig. 3 enables us to compare nanofabricated structures of different dimensions in terms of their surface temperature as a result of rapid laser heating. Based on these findings, we can predict the fluence levels necessary to reach similar ion emission conditions as well as similar surface temperatures for structures with different dimensions, resulting in a broad applicability for the method. For example, for $D = 300$ nm posts the fluence level to reach similar temperatures is $F = 139$ in arbitrary units.

Although (5) establishes a correlation between surface temperatures and the $[MNa^+]/[MK^+]$ ratio, most parameters necessary to obtain absolute temperature values are not known. Even if the activation energies and the frequency factors for silicon become available, most nanostructures are heterogeneous (see the chromium caps in the NAPA), so the values for silicon might not be appropriate. To determine the Arrhenius parameters for a particular structure, temperature distribution modeling along with the observation of transient melting can lead to more accurate relative temperatures.

3.2 Temperature distribution modeling

For pure diffusive heat transport laser heating of nanoposts was followed by solving (1) with the appropriate boundary conditions. Surface temperatures were calculated at the end of a 5 ns nitrogen laser pulse for fluences between 10 and 100 mJ/cm^2. These fluences fell into the range used in laser desorption ionization experiments on silicon nanowire and laser induced silicon microcolumn array (LISMA) [19] substrates, and in desorption ionization on porous silicon (DIOS) [20]. Except for low fluences, the correlation between the surface temperature and the fluence was close to linear. As the post diameter was reduced from 250 nm to 50 nm, the slope of the temperature-fluence curve increased. Using the same fluence thinner posts reached higher temperatures than their thick counterparts. This effect stems from radial energy confinement in the posts when their diameter falls below the heat diffusion length. A consequence of this phenomenon was observed in Fig. 1b indicating similar ion yields for 100 nm and 200 nm posts at significantly higher fluences for the latter.

The thermal diffusivity is a strong function of the temperature. For un-doped silicon at room temperature $\kappa = 0.8$ cm^2/s but this value drops to $\sim$0.1 cm^2/s above 1000 K. This means that the thermal diffusion length for the 5 ns laser pulse, $2(\kappa t)^{1/2}$, drops to $\sim$400 nm, which is comparable to the studied post diameters.

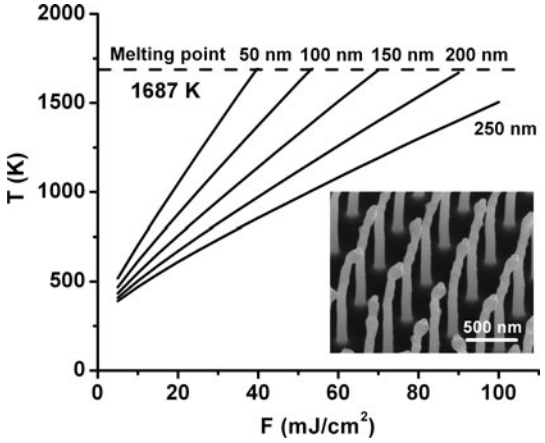

Fig. 4 Calculated surface temperatures of nanoposts as a function of fluence indicate that, when using the same fluence, thinner posts reach higher temperatures than their thick counterparts. Consequently, thinner posts reach the melting temperature at lower fluences. The inset shows the deformation of $D = 100$ nm nanoposts observed by SEM, indicating transient melting as temperatures exceed the melting temperature of silicon. The NAPA post heights and periodicities were $H = 1000$ nm and $P = 400$ nm, respectively

Another consequence of energy confinement was that the thinner posts reached the melting temperature at lower fluences (see Fig. 4). For example, $D = 50$, 100 and 200 nm posts reached the silicon melting temperature at $F = 39.8$, 53.2 and 92.0 mJ/cm^2, respectively. Transient melting of thinner posts (see the inset in Fig. 4 for the $D = 100$ nm case) and $D = 50$ nm nanowires [3] was, indeed, observed by SEM in laser desorption ionization experiments using similar fluences. These results also support the use of the diffusive heat transport model. Although the post diameters are below the estimated 800 nm phonon mean free path, the diffusive transport model still seems to correctly predict the melting of the thin structures and the lack of melting for the thicker posts in typical laser desorption ionization experiments.

Combining alkali ion yield ratio and absolute fluence measurements with validated surface temperature calculations can go a long way to establish a high throughput heating load assessment method for the laser heating of nanostructures.

Acknowledgements This research was funded by The Chemical Sciences, Geosciences and Biosciences Division within the Office of Basic Energy Sciences of the US Department of Energy (Grant DE-FG02-01ER15129) and by the George Washington University Research Enhancement Fund (GWU-REF). Scholarship awards from the Achievement Rewards for College Scientists Foundation, Inc. (ARCS) to B.N.W. and J.A.S. and support from Protea Biosciences, Inc. to B.N.W. are greatly appreciated. NAPA structures were nanofabricated in the framework of a User Agreement (CNMS2008-249) at Oak Ridge National Laboratory's Center for Nanophase Materials Sciences, sponsored by the Scientific User Facilities Division, Office of Basic En-

ergy Sciences, US Department of Energy. Instrument maintenance by T. Hawley of the George Washington University supported the mass spectrometry experiments.

References

1. J.P. Wisniewski, M. Clampin, K.S. Bjorkman, R.K. Barry, Astrophys. J. Lett. **683**, L171 (2008)
2. J.W. Ahn, R. Maingi, D. Mastrovito, A.L. Roquemore, Rev. Sci. Instrum. **81**, 4 (2010)
3. G.H. Luo, Y. Chen, H. Daniels, R. Dubrow, A. Vertes, J. Phys. Chem. B **110**, 13381 (2006)
4. A. Majumdar, J. Heat Transfer Trans. Asme **115**, 7 (1993)
5. A.A. Joshi, A. Majumdar, J. Appl. Phys. **74**, 31 (1993)
6. W.J. Liu, M. Asheghi, J. Heat Transfer Trans. Asme **128**, 75 (2006)
7. D.Y. Li, Y.Y. Wu, P. Kim, L. Shi, P.D. Yang, A. Majumdar, Appl. Phys. Lett. **83**, 2934 (2003)
8. K. Moller, L. Holmlid, Surf. Sci. **179**, 267 (1987)
9. M. Hagstrom, K. Engvall, J.B.C. Pettersson, J. Phys. Chem. B **104**, 4457 (2000)
10. G.J.Q. Vanderpeyl, K. Isa, J. Haverkamp, P.G. Kistemaker, Org. Mass Spectrom. **16**, 416 (1981)
11. G.J.Q. Vanderpeyl, K. Isa, J. Haverkamp, P.G. Kistemaker, Nucl. Instrum. Methods Phys. Res. **198**, 125 (1982)
12. G. Wedler, H. Ruhmann, Surf. Sci. **121**, 464 (1982)
13. B.N. Walker, J.A. Stolee, D.L. Pickel, S.T. Retterer, A. Vertes, J. Phys. Chem. C **114**, 4835 (2010)
14. M. von Allmen, A. Blatter, *Laser-Beam Interactions with Materials* (Springer, Berlin, 1995)
15. J.S. Heron, T. Fournier, N. Mingo, O. Bourgeois, Nano Lett. **9**, 1861 (2009)
16. H.M. Branz, V.E. Yost, S. Ward, K.M. Jones, B. To, P. Stradins, Appl. Phys. Lett. **94**, 3 (2009)
17. Y. Chen, A. Vertes, Anal. Chem. **78**, 5835 (2006)
18. Z. Olumee, A. Vertes, J. Phys. Chem. B **102**, 6118 (1998)
19. J.A. Stolee, Y. Chen, A. Vertes, J. Phys. Chem. C **114**, 5574 (2010)
20. G.H. Luo, Y. Chen, G. Siuzdak, A. Vertes, J. Phys. Chem. B **109**, 24450 (2005)